Voltage Tunability of Quantum Cascade Lasers

Yu Yao, Zhijun Liu, Anthony J. Hoffman, Kale J. Franz, *Student Member, IEEE*, and Claire F. Gmachl, *Senior Member, IEEE*

***Abstract*—The voltage tunability of three types of quantum cascade laser designs is investigated. The tuning coefficients and tuning ranges of electroluminescence and laser emission from all designs are measured and compared with the calculated results. A reduced tunability was observed in all lasers above threshold. This is attributed to the decrease of resistance across the laser active region (AR) as the photon density increases. A resumed tunability high above threshold occurs in all lasers with anticrossed injector ground and upper laser states. Lasers based on the anticrossed diagonal transition are tunable above threshold, with a tuning range of about 30 cm^{-1} ($\sim$3% of the laser emission wavenumber), i.e., a tuning rate of 750 $cm^{-1}V^{-1} \cdot period^{-1}$ of the AR and the injector.**

***Index Terms*—Quantum cascade (QC) lasers, Stark effect, tunable lasers.**

I. Introduction

QUANTUM CASCADE (QC) lasers are ideal candidates for midinfrared spectroscopy because their emission wavelength can be designed in the mid-to-far-infrared range from 2.7 to 24 μm [1], [2]. A broad wavelength tuning range is required for lasers in many applications. In the detection of multiple trace gases or chemical species with interfering absorption features, for example, it is necessary to tune the laser wavelength over a wide range. Broad tunability requires a gain medium that can provide gain over a wide wavelength range. Heterogeneous active regions [3] (ARs) or bound-to-continuum designs [4] can be used to achieve a broader gain spectrum. However, both come at the cost of the peak gain. An alternative method would be a widely tunable gain spectrum.

Voltage tuning of QC lasers based on a strong linear Stark effect in quantum wells is expected to function at a much higher tuning speed than the temperature tuning. The tuning coefficient is proportional to the spatial distance between the centroids of the electron probability distributions of the upper and lower laser states [5]. Theoretically, one can achieve very large tuning coefficients by increasing the spatial distance between the two states. Faist *et al.* [6] demonstrated a broad tuning range of the intersubband electroluminescence (EL) (over 220 cm^{-1}) in a structure based on photon-assisted tunneling. However, above threshold, the lasers are not tunable.

In this paper, we investigated the voltage tunability of the prevailing QC laser designs based on anticrossed vertical and diagonal transitions, which have the best performance in room temperature continuous-wave (CW) operation. Both designs make use of resonant tunneling to inject electrons from the injector ground state into the upper laser state. We also compare these designs with a sample based on a photon-assisted diagonal transition AR. The paper is arranged as follows. Section II gives a detailed explanation of the experiments. Section III discusses the tunability of intersubband EL, comparing the measured and calculated results. In part IV, the tunability of lasers of all three designs is studied. All lasers have reduced tunability above threshold; however, lasers based on an anticrossed diagonal transition AR can be tuned over 30 cm^{-1} (3% of the laser emission wavenumber) above threshold with a tuning coefficient of 750 $cm^{-1}V^{-1}period^{-1}$ of the AR and the injector because of a resumed tunability. Section V is the conclusion.

II. Experiment

The samples studied in this paper are based on three different types of QC laser designs. Fig. 1(a) shows an anticrossed vertical transition design (sample AVQ) [7]. Fig. 1(b) is an anticrossed diagonal transition design (sample ADQ) [8]. Both of them are widely used at present in achieving high-performance QC lasers. Fig. 1(c) shows a diagonal transition design based on photon-assisted tunneling ("super" diagonal design, sample SDQ) [9]. All three samples were processed into 200-μm-diameter circular mesas. The mesas were etched past the active core with slanted side walls to ensure that the EL would not be impacted by any cavity effect; for each sample, ridge lasers were also processed for different threshold current densities by changing the width and the length of the laser cavity. All lasers are based on a Fabry–Perot (FP) cavity with as-cleaved facets. The EL from the mesas was measured at low temperature (80 K) in pulsed mode (100-ns pulse width, 80 kHz) using a Fourier-transform infrared spectrometer (FTIR) with a cooled HgCdTe (MCT) detector. The EL of lasers below threshold and laser spectra above threshold were also measured at the same condition. The low temperature and small duty cycle ensure that the measured results are not impacted by thermal effects.

The peak wavenumber of the EL can be determined by fitting the raw data with (if necessary, multiple) Gaussian or Lorentzian peaks and selecting the peak value of the fitted curve, as shown in Fig 2(a). The asymmetry of the EL is because of multiple optical transitions that co-occur in the quantum well structures.

Manuscript received August 20, 2008; revised September 26, 2008. Current version published May 20, 2009. This work was supported in part by Mid-InfraRed Technologies for Health and the Environment (MIRTHE) [National Science Foundation (NSF) Engineering Research Council (ERC)] and in part by the Defense Advanced Research Projects Agency (DARPA) Efficient Midwave Infrared Laser (EMIL).

Y. Yao, A. J. Hoffman, K. J. Franz, and C. F. Gmachl are with the Department of Electrical Engineering and the Princeton Institute for the Science and Technology of Materials, Princeton University, Princeton, NJ 08544 USA (e-mail: yuyao@princeton.edu; ajhoffma@princeton.edu; kfranz@princeton.edu; cgmachl@princeton.edu).

Z. Liu is with the Division of Engineering, Brown University, Providence, RI 02912 USA (e-mail: zhijunlcy@hotmail.com).

Color versions of one or more of the figures in this paper are available online at http://ieeexplore.ieee.org.

Digital Object Identifier 10.1109/JQE.2009.2013122

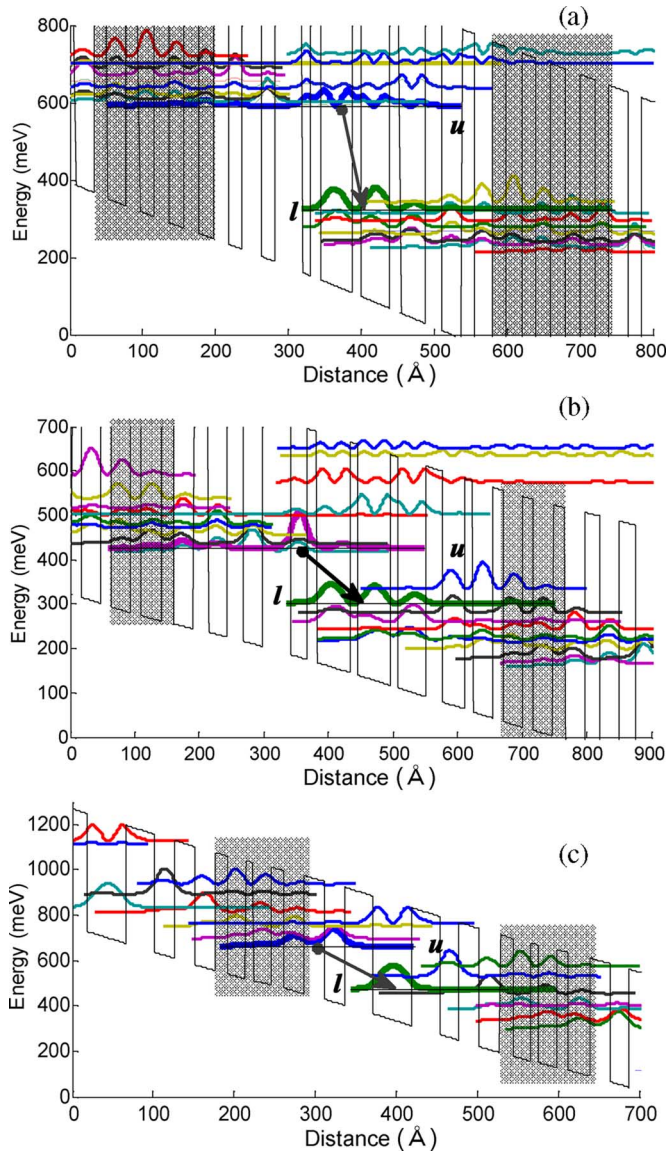

Fig. 1. Conduction band diagram of a portion of the ARs and injectors and the moduli squared of the relevant wave functions of (a) sample AVQ under an average electric field of 75 kV/cm, (b) sample ADQ under an average electric field of 43 kV/cm, and (c) sample SDQ under an average electric field of 100 kV/cm. The bold curves represent the upper and lower laser states. The arrows indicate the respective laser transitions. The shaded regions indicate the doped layers. All structures are calculated with a self-consistent Poisson–Schrödinger solver.

Fig. 2(b) shows the spectra of a laser based on the anticrossed diagonal design (sample ADQ) at different injection current densities. The wavenumbers of the lasing spectra are around the main peak of the EL, which corresponds to the transition between the upper and lower laser states. The spectrum broadens as the current density increases, splitting into two or three humps when the driving current exceeds a certain value. This phenomenon was found in most of the lasers measured in our study.

The broadening of the laser spectra has several reasons: spatial hole burning, Rabi splitting [10], and wavelength-dependent loss (introduced by material defect or waveguide nonuniformity, e.g.). To determine the tuning trend of the laser spectra, we measured the wavenumbers on both sides at half-height of

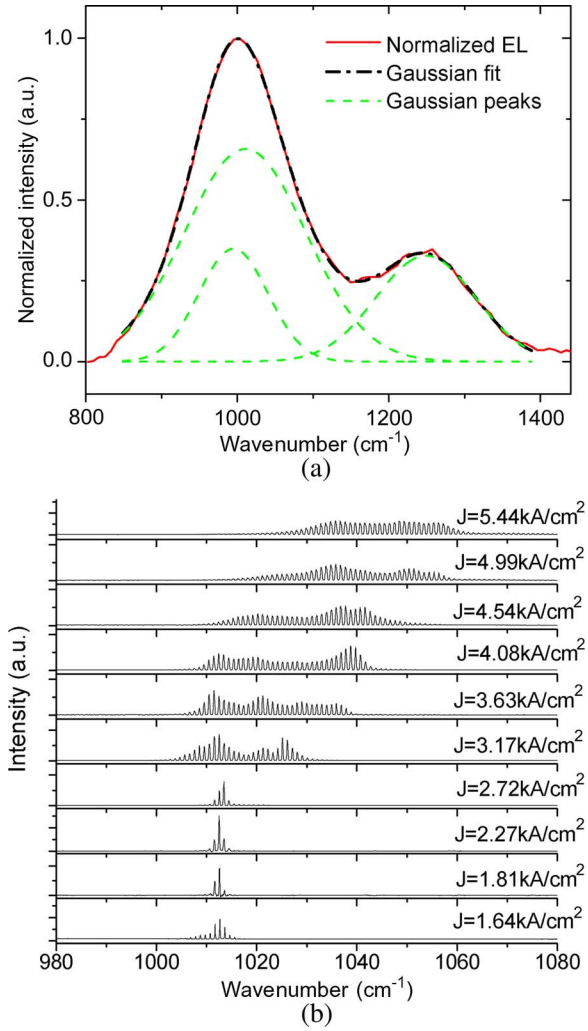

Fig. 2. (a) EL from a mesa based on the anticrossed diagonal design (sample ADQ). (b) Spectra of a laser (sample ADQ) at different injection current densities. Both graphs are taken at $T = 80$ K in pulsed mode.

the peak intensity and extracted the midpoint value for the laser wavenumber. This method gives consistent results for lasers based on the same design.

III. Voltage Tunability of EL

As mentioned previously, the voltage tuning of the intersubband EL is a consequence of the linear Stark effect in the quantum wells. The EL tuning coefficient is proportional to the spatial distance between the two transition states [5], [6]

$$\frac{dE_{\rm ph}}{dF} = q(z_l - z_u) \tag{1}$$

where $E_{\rm ph}$ is the transition energy, F is the electrical field in the AR, q is the electron charge, and z_l, z_u are the coordinates of the centroids of the electron probability distributions at the lower and upper laser states, respectively. The electron probability distributions change with applied electric fields. Therefore, we employ a self-consistent Poisson–Schrödinger solver to calculate the band structure at different electric fields, considering

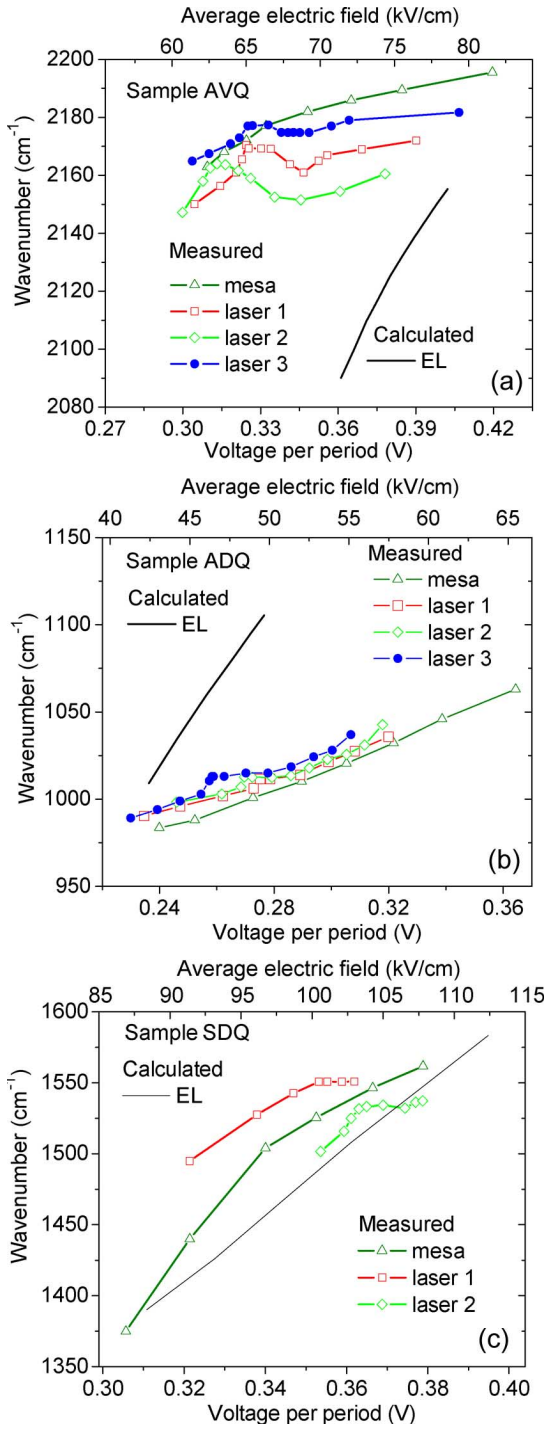

Fig. 3. (a) Anticrossed vertical design (sample AVQ). (b) Antirossed diagonal design (sample ADQ). (c) "Super" diagonal design (sample SDQ). Calculated peak EL wavenumber (solid lines) and measured peak EL and laser emission wavenumbers (symbols) as functions of the voltage drop per period of the AR and the injector (bottom axis) and the average electric field (top axis). All experimental data are measured at 80 K in pulsed mode.

the impact of electron distribution on the local electric field according to the Gauss law. The results are shown in Fig. 3(a)–(c) for the anticrossed vertical design, anticrossed diagonal design, and ''super'' diagonal design, respectively.

The measured EL peak wavenumbers of mesas are also shown in Fig. 3 as functions of the voltage drop over each period of the AR and the injector for all three structures. The corresponding average electric field over the injectors and ARs is also given on the top axes. The tuning coefficient can be calculated as

$$\frac{dE_{\rm ph}}{dF_{ave}} = \frac{dE_{\rm ph}}{dV_p} L_p \tag{2}$$

where V_p is the voltage over one period, L_p is the length of one period, and $F_{\rm ave}$ is the average electric field over the AR and the injector in the core of the QC laser structure. Both calculated and measured EL tuning coefficients for all three samples are shown in Table I. The measured results show that the "super" diagonal design has the largest tuning coefficient, followed by the anticrossed diagonal design, while the anticrossed vertical design has the smallest tuning coefficient. However, the calculated results show the largest tuning coefficient for the anticrossed diagonal design and the smallest tuning coefficient for the "super" diagonal design. This overestimation of tuning coefficients for the anticrossed designs has also been found by Müller *et al.* [11].

TABLE I
TUNING COEFFICIENTS OF ELECTROLUMINESCENCE

Sample	Measured (cm^{-1} per kV/cm)	Calculated (cm^{-1} per kV/cm)
AVQ (Anti-crossed vertical)	1.04 (V_p>0.332V) 3.06 (V_p<0.332V)	8.98
ADQ (Anti-crossed diagonal)	3.76	13.2
SDQ ("Super" diagonal)	5.21 (V_p>0.34V) 13.17 (V_p<0.34V)	8.12

For the anticrossed vertical and diagonal designs, the upper and lower laser states are widely distributed across the quantum wells when they come into anticrossing with the injector states, which results in a very large spatial distance between the upper and lower laser states. However, because of various scattering mechanisms that are not included in the calculation, the electron probability distributions are more localized than calculated. If we take this into consideration, a smaller spatial distance is expected. Therefore, the real tuning coefficients are smaller than the calculated results.

We also notice that for some designs, the tuning coefficients change with the applied voltage. For example, the anticrossed vertical design has a much larger tuning coefficient for an applied voltage per period below 0.33 V than for the voltage above that. The likely reason is the electron screening, as mentioned in [6]. When the applied voltage is low, more and more extrinsic electrons from the doped region relax to the injection barrier as the voltage is increased. As a result, the positive charge in the doped region and the extrinsic electrons generate a stronger built-in electric field, which is in the opposite direction to the applied field. This leads to a smaller increase of electric field in the injectors but a larger increase of electrical field in the AR. In the following, this voltage range will be referred as the screening region. When the voltage is large enough, most of the electrons are accumulated in front of the injection barrier. A further increase in voltage will lead to little change in the electron distribution.

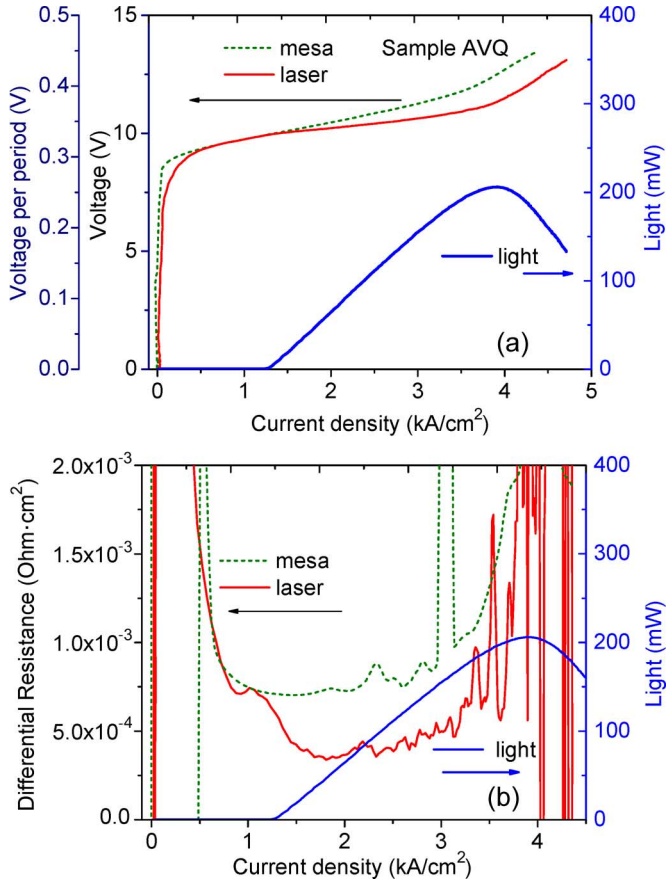

Fig. 4. (a) Voltage versus current density (*JV*) characteristics and (b) differential resistance (dV/dJ) for lasers and mesas based on anticrossed vertical design (sample AVQ), measured at $T = 80$ K in pulsed mode.

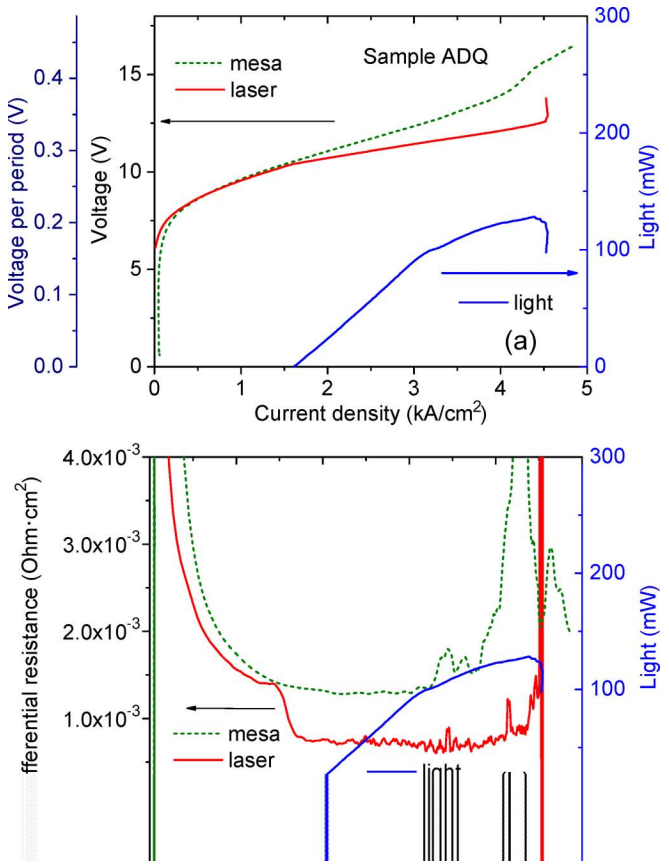

Fig. 5. (a) Voltage versus current density (*JV*) characteristics and (b) differential resistance (dV/dJ) (b) for lasers and mesas based on anticrossed diagonal design (sample ADQ), measured at $T = 80$ K in pulsed mode.

Therefore, only above the screening region, the change in the electric field and the voltage over one period are linearly related

$$dF = \frac{dV_p}{L_p} = dF_{\text{ave}} \tag{3}$$

which means that the increase of voltage will result in uniform increase of the electric field over the AR and injector, even though the electric field is not uniform.

The measured results show an EL tuning range of about 40 cm^{-1} for the anticrossed vertical design (AVQ), 90 cm^{-1} for the anticrossed diagonal design (ADQ), and 190 cm^{-1} for the "super" diagonal design (SDQ), i.e., 2%, 9%, and 12.5% of their EL peak wavenumbers, respectively. The diagonal designs have much larger tuning ranges as well as tuning coefficients than the vertical design, certainly because of a larger spatial distance. This spatial distance can be made larger by engineering the band structure or reducing the scattering in quantum wells.

IV. Voltage Tunability of Lasers

The peak wavenumbers of the laser spectra are also shown in Fig. 3. All the lasers are tunable below threshold. However, their tunability is reduced above threshold. For the anticrossed vertical design, the wavenumbers decrease first and then start increasing again after a certain voltage (0.35 V for sample AVQ). For lasers based on the anticrossed diagonal design, the wavenumbers are almost constant just above threshold, but the tunability approaches that of the EL after the voltage over one period is higher than 0.28 V. Lasers based on the "super" diagonal design have almost no tuning above threshold. Since the lasers and mesas are made from the same wafers, they have identical active cores (ARs and injectors) and waveguide structures. The most significant difference between lasers and mesas is that the stimulated emission strongly influences the lasers' optical and electrical behavior above threshold. The discontinuity of the differential resistance at threshold has been found in QC lasers [12]. The reason lies in the stimulated emission. Here, we compare the current density–voltage (*JV*) curves as well as differential resistances of mesas and lasers, as shown in Figs. 4–6, respectively. The voltage is obtained by subtracting from the raw data the voltage over an "empty" structure (a QC laser structure including everything except the active core).

For all three designs, the voltage over the laser active core becomes smaller than that of the mesas above threshold. The differential resistances are calculated by differentiating the *JV* curves. The experimental results show that all the lasers experience a drop in differential resistance at threshold, while the differential resistance of mesas is continuous.

An understanding of these observations can be achieved by analyzing the effect of the stimulated emission on the AR.

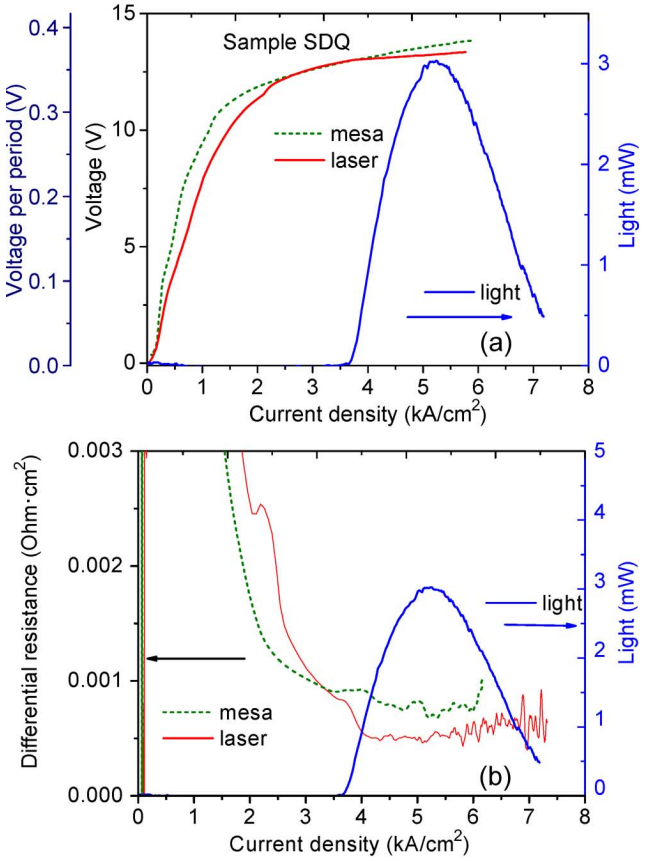

Fig. 6. Voltage versus current density (*JV*) characteristics (a) and differential resistance (dV/dJ) (b) for lasers and mesas based on "super" diagonal design (sample SDQ), measured at $T = 80$ K in pulsed mode.

Starting from the rate equation of the electron population in the upper laser state,

$$\frac{dN_u}{dt} = R_u - \frac{N_u}{\tau_u} - \sigma \Delta N \varphi \tag{4}$$

where N_u, ΔN are the population on the upper laser state and the population inversion between the upper and the lower laser states, respectively; R_u is the electron pumping rate into the upper laser state; τ_u is the phonon scattering lifetime of the upper laser state; σ is the gain cross section and φ is the photon flux in the cavity.

Below threshold, the stimulated emission (the third term on the right in (4)) can be omitted. However, above threshold, a large portion of the electrons at the upper laser state will transit to the lower laser state via stimulated emission, which results in faster depopulation of the upper laser state. If we include the stimulated emission term into the second term in (4), we can define an effective lifetime for the upper laser state, τ_u^{eff}:

$$\frac{1}{\tau_u^{\text{eff}}} = \frac{1}{\tau_u} + \frac{\Delta N}{N_u}\sigma\varphi \tag{5}$$

$$\frac{dN_u}{dt} = R_u - \frac{N_u}{\tau_u^{\text{eff}}}. \tag{6}$$

Above threshold, the light intensity in the cavity is increased as the injection current increases. Therefore, the effective lifetime of the upper laser state becomes smaller, according to (5). This has been verified in the femtosecond time-resolved pump-probe measurement recently by Choi *et al.* [13].

The decrease of the effective lifetime of the upper laser state results in a reduced resistance in the AR, i.e., as the light intensity inside the cavity becomes stronger and stronger, more and more electrons transit across the AR via stimulated emission. The AR allows more current to pass even if the voltage across it does not change. Therefore, when the current density goes up, most of the voltage increase is across the injectors; the electrical field in the AR does not grow as fast.

If we omit the impact of stimulated emission on the electrical property of the injectors, which should be much less than that on the ARs, we can regard the voltage on the mesa injectors the same as the voltage on the laser injectors at the same current density. The difference between *JV* characteristics of the lasers and mesas is attributed to a voltage decrease across the ARs because of the stimulated emission. Given the *JV* curves of the mesas and lasers, we can then calculate the decrease of voltage over the ARs in the lasers compared with mesas

$$\delta V(J) = V_m(J) - V_l(J) \tag{7}$$

where $V_m(J)$ and $V_l(J)$ are the voltage on mesas and lasers at the current density J, respectively. For simplicity, we assume that the voltage change over the AR is uniformly distributed, since the electron population inversion is constant above threshold. Therefore, the decrease of the electric field over the AR in each period can be calculated as

$$\delta E_{\text{AR}}(J) = \frac{\delta V(J)}{L_{\text{AR}} N_p} \tag{8}$$

where L_{AR} is the length of the AR and N_p is the number of periods in the core of the QC laser structure. By multiplying the measured EL tuning coefficients with the decrease of the electrical field over the AR, we can calculate the change in wavenumbers for the lasers compared with the EL peaks of the mesas made from the same sample

$$\delta\left(\frac{1}{\lambda}\right) = \frac{L_p d\left(\frac{1}{\lambda}\right)}{dV_p}\delta E_{\text{AR}} \tag{9}$$

where λ is the emission wavelength. Note that this method only applies above the carrier screening region, as discussed before.

The calculated results for the "super" diagonal design (SDQ) and the anticrossed diagonal design (ADQ) are shown in Fig. 7. For the "super" diagonal design, the calculated results match very well with the experimental results. For the anticrossed diagonal design, the calculated results show that lasers have almost no tunability above threshold. This explains the measured results just above threshold. However, the laser wavenumbers start growing as fast as that of the EL after a certain voltage ($V_p = 0.28$ V for sample ADQ), as shown in Fig. 3(a), which cannot be explained by our model.

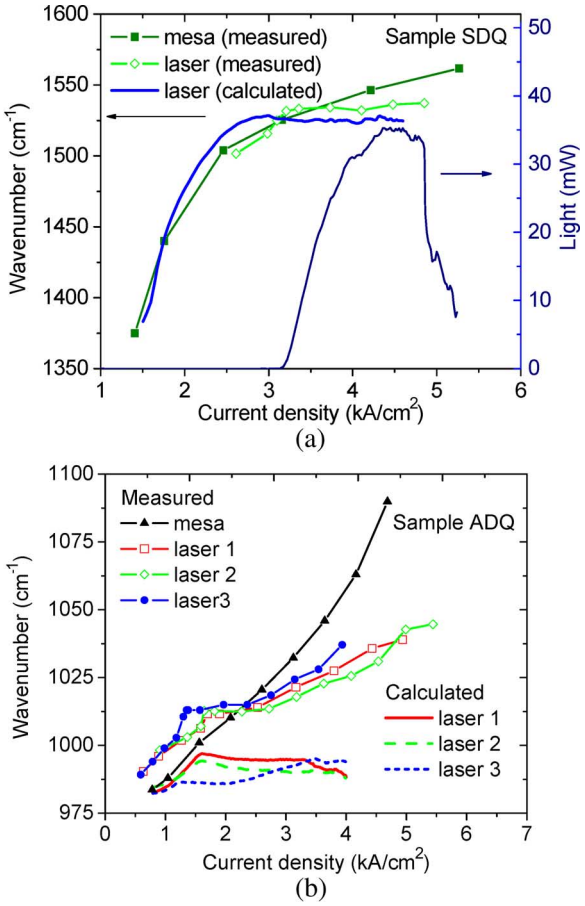

Fig. 7. Solid lines: calculated peak emission wavenumbers of lasers taking into account the impact of stimulated emission on the electrical field over the AR in the lasers. Symbols: measured wavenumbers of mesa EL peaks as well as laser EL below threshold and laser spectra above threshold as a function of the current density for (a) the "super" diagonal design [sample SDQ, laser 2 of Fig. 3(c)] and (b) the anticrossed diagonal design (sample ADQ). All experimental results are taken at 80 K in pulsed mode.

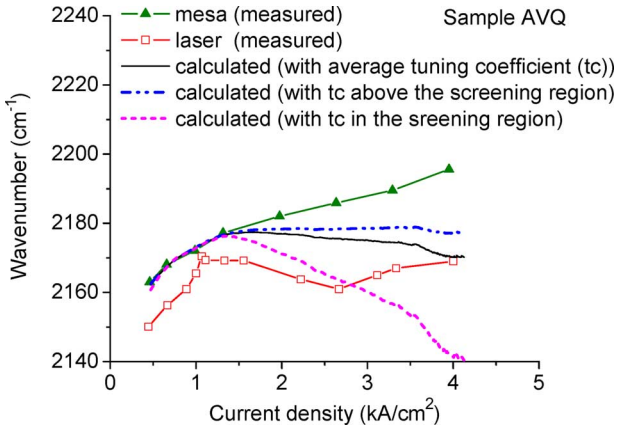

Fig. 8. Anticrossed vertical design (sample AVQ). Lines: calculated peak emission wavenumbers of a representative laser [laser 1 of Fig. 3(a)] taking into account the impact of stimulated emission on the electrical field over AR in lasers. Symbols: wavenumbers of mesa EL peaks as well as laser EL below threshold and laser spectra above threshold as a function of the current density. All experimental results are taken at 80 K in pulsed mode.

As for the anticrossed vertical design (sample AVQ), the laser thresholds are in the carrier screening region, where the increase of the electric field is not uniform over the AR and the injector. Therefore, it is very difficult to extract the tuning coefficients of the EL peak wavenumbers versus electrical field over the AR. The tuning coefficients calculated from the measured EL wavenumbers are larger than the real tuning coefficients since the electrical field over the AR increases faster than that of the average electrical field. One extreme is that all the voltage increase is over the AR, the real tuning rate is then 1.35 cm^{-1} per kV/cm, which is higher than the tuning coefficient above the screening region (1.04 cm^{-1} per kV/cm). Therefore, the average real tuning coefficient is between the tuning coefficients for the carrier screening region and that for the region above. Fig. 8 shows the calculated emission wavenumbers for one representative laser of sample AVQ, using the tuning coefficients for the screening region and the region above, respectively. The real case lies in between the two curves, e.g., the solid line in Fig. 8 shows the calculated result using the tuning coefficient obtained by fitting the data (EL peak wavenumbers versus the average electrical field) in the whole electrical field range. Compared with the measured results, the reduced tunability above threshold can be explained. Moreover, the laser wavenumbers may decrease as the applied voltage increases, which indicates the decrease of voltage over AR because of its reduced resistance. Similar to the anticrossed diagonal design, the calculation cannot explain the resumed tunability of lasers above a certain voltage ($V_p = 0.35$ V for sample AVQ).

Based on the results for the anticrossed designs (sample ADQ and AVQ) and the "super" diagonal design (sample SDQ), we found that the resumed tunability occurs only for the anticrossed designs. Different lasers of the same sample start to be tunable again above the same voltage. We attribute this to the anticrossing between the injector state and the upper laser state. When the ground state of the upstream injector comes into strong anticrossing with the upper laser state, it acts as a lever on the upper laser state as the electrical field in the injector is increased. Because of this resumed tunability, lasers based on the anticrossed diagonal transition are tunable above threshold, with a tuning range around 30 cm^{-1} (3% of the laser emission wavenumber) and a tuning coefficient of 3.7 cm^{-1} per kV/cm.

V. Conclusion

The voltage tunability of intersubband EL is mainly determined by the spatial difference of the upper and lower laser states. The tuning ranges for the 'super' diagonal, anticrossed diagonal, and anticrossed vertical design are 190, 90, and 40 cm^{-1}, i.e., 12.5%, 9%, and 2% of their EL peak wavenumbers, respectively. The comparison of measured and calculated tuning coefficients shows a large overestimation for designs based on resonant tunneling. The explanation is that the scattering in quantum wells (because of roughness, impurities, etc.) results in more localized electron probability distributions and therefore, leads to a smaller tuning coefficient than calculated.

Lasers above threshold show a different tunability from the EL. The stimulated emission leads to the drop of resistance at threshold in lasers. Moreover, the dramatic increase of light intensity above threshold makes the resistance of the AR decrease as the current density increases. Thus, the electric field over the

AR does not increase as much as that over the injectors. To validate this explanation, we presented the calculated results for laser wavenumbers based on the measured current–voltage characteristics of mesas and lasers as well as measured EL tuning coefficients.

A resumed tunability has been observed in anticrossed designs. A comparison of the results of the anticrossed designs with that of the "super" diagonal design suggests that this is due to the anticrossing of the ground state in the injector with the upper laser state. Lasers based on anticrossed diagonal transition have a tuning range of about 30 cm^{-1} (3% of the laser emission wavenumber) above threshold and a tuning coefficient of 750 $cm^{-1}V^{-1}period^{-1}$ of the AR and the injector.

ACKNOWLEDGMENT

The authors would like to thank X. Wang and J. Fan at AdTech Optics, City of Industry, CA, F. J. Towner at Maxion Technologies, Inc., Hyattsville, MD, and D. L. Sivco at Alcatel-Lucent, Murray Hill, NJ for wafer growth.

REFERENCES

[1] C. Gmachl, F. Capasso, D. L. Sivco, and A. Y. Cho, "Recent progress in quantum cascade lasers and applications," *Rep. Prog. Phys.*, vol. 64, pp. 1533–1601, 2001.

[2] R. Teissier, J. Devenson, O. Cathabard, and A. N. Baranov, "Short wavelength quantum cascade lasers emitting around 3 μm," presented at the in Proc. Conf. Lasers Electro-Opt., San Jose, CA, May 4–9, 2008, .

[3] C. Gmachl, D. L. Sivco, R. Colombelli, F. Capasso, and A. Y. Cho, "Ultra-broadband semiconductor laser," *Nature*, vol. 415, pp. 883–887, Feb. 2002.

[4] J. Faist, M. Beck, T. Aellen, and E. Gini, "Broadband tuning of external cavity bound-to-continuum quantum-cascade lasers," *Appl. Phys. Lett.*, vol. 84, pp. 1659–1661, Mar. 2004.

[5] P. F. Yuh and K. L. Wang, "Large stark effects for transitions from local states global states in quantum well structures," *IEEE J. Quantum Electron*, vol. 25, no. 7, pp. 1671–1676, Jul. 1989.

[6] J. Faist, F. Capasso, C. Sirtori, D. L. Sivco, A. L. Hutchinson, and A. Y. Cho, "Laser action by tuning the oscillator strength," *Nature*, vol. 387, pp. 777–782, Jun. 1997.

[7] A. Evans, J. S. Yu, S. Slivken, and M. Razeghi, "Continuous-wave operation of $\lambda \sim 4.8$ μm quantum-cascade lasers at room temperature," *Appl. Phys. Lett.*, vol. 85, pp. 2166–2168, 2004.

[8] Z. Liu, C. F. Gmachl, L. Cheng, F. Choa, F. J. Towner, X. Wang, and J. Fan, "Temperature-dependent gain and loss in room-temperature continuous-wave quantum cascade lasers between 8.2–10.3 μm," *IEEE J. Quantum Electron*, vol. 44, no. 5, pp. 485–492, May 2008.

[9] C. Gmachl, A. Tredicucci, D. L. Sivco, A. L. Hutchinson, F. Capasso, and A. Y. Cho, "Bidirectional semiconductor laser," *Science*, vol. 286, pp. 749–752, Oct. 1999.

[10] C. Y. Wang, L. Dieh, A. Gordon, C. Jirauschek, F. X. Kärtner, A. Belyanin, D. Bour, S. Corzine, G. Höfler, M. Troccoli, J. Faist, and F. Capasso, "Coherent instabilities in a semiconductor laser with fast gain recovery," *Phys. Rev. A*, vol. 75, pp. 031802-1(R)–031802-4(R), 2007.

[11] A. Müller, M. Beck, J. Faist, U. Oesterle, and M. Ilegems, "Electrically tunable, room-temperature quantum-cascade lasers," *Appl. Phys. Lett.*, vol. 75, no. 11, p. 1509, 1999.

[12] C. Sirtori, F. Capasso, J. Faist, A. L. Hutchinson, D. L. Sivco, and A. Y. Cho, *Reson. Tunnel. Quantum Cascade Lasers*, vol. 34, no. 9, pp. 1722–1729, Sep. 1998.

[13] H. Choi, L. Diehl, Z. Wu, M. Giovannini, J. Faist, F. Capasso, and T. B. Norris, "Gain recovery dynamics and photon-driven transport in quantum cascade lasers," *Phys. Rev. Lett.*, vol. 100, no. 16, pp. 167401-1–167401-4, Apr. 2008.

Yu Yao received the B.S. and M.S. degrees in electrical engineering from Tsinghua University, Beijing, China, in 2004 and 2006, respectively. She is currently working toward the Ph.D. degree at the Department of Electrical Engineering, Princeton University, Princeton, NJ.

Her current research interests include high-performance quantum-cascade lasers.

Zhijun Liu received the B.S. and M.S. degrees in physics from Sichuan University, Chengdu, China, in 2000 and 2003, respectively, and the Ph.D. degree in electrical engineering from Princeton University, Princeton, NJ, in 2008. His doctoral research focused on high-performance quantum cascade lasers for sensins applications.

Since October 2008, he has been with the Division of Engineering, Brown University, Providence, RI, as a Postdoctoral Research Associate. His current research interests include subwavelength lasers and lead salt infrared materials and devices.

Anthony J. Hoffman received the B.S. degree in physics (with honors) from the University of Maryland Baltimore County in 2004 and the Ph.D. degree in electrical engineering from Princeton University, Princeton, NJ, in 2009. His doctoral work was on high-performance quantum cascade lasers and mid-infrared materials.

He is currently a Postdoctoral Research Associate with Princeton University, where he is working on circuit quantum electrodynamics.

His current research interests include quantum cascade lasers and midinfrared negative index of refraction materials.

Kale J. Franz (S'05) received the B.S. degree in engineering physics (with Highest Scholastic Honors) from the Colorado School of Mines, Golden, in 2004 and the Ph.D. degree in electrical engineering from Princeton University, Princeton, NJ, in 2009.

While at Princeton, his research focused on improving the capabilities and performance of quantum cascade laser technology. From 2001 to 2002, he was an Intern with the U.S. Department of Energy Office of Science, working on science and education policy initiatives. From 2003 to 2004, he performed in research on the growth and fabrication of carbon nanotubes, for the primary application of hydrogen storage. He has authored or coauthored more than 15 publications and conference proceedings along with 28 presentations and holds three patents and provisional applications. While at Princeton, he was supported by a National Science Foundation Graduate Research Fellowship, and he is currently Princeton University Wallace Fellow.

Dr. Franz is currently serving a term as the IEEE Princeton/Central New Jersey Photonics (formerly the Lasers and Electro-Optics Society) Society Section Chapter Chair.

Claire F. Gmachl (S'94–A'95–SM'00) received the Ph.D. degree (*sub auspicies praesidentis*) in electrical engineering from the Technical University of Vienna, Vienna, Austria, in 1995.

In 1996, she joined Bell Laboratories, Lucent Technologies, Murray Hill, NJ, as a Postdoctoral Member of Technical Staff, where she was engaged in the research on quantum cascade laser devices and microcavity lasers. In March 1998, she became a Member of Technical Staff in the Semiconductor Physics Research Department and a Distinguished Member of the Staff in 2002. In September 2003, she became an Associate Professor in the Department of Electrical Engineering and an Adjunct Faculty to PRISM at Princeton University, Princeton, NJ, where she is currently a Full Professor since 2007 and the Director of the MidInfraRed Technologies for Health and the Environment (MIRTHE), the National Science Foundation Engineering Research Center on MIRTHE formed in 2006. She has authored or coauthored more than 170 publications, has given more than 100 presentations at conferences and seminars, and holds 26 patents. She is an Associate Editor of the *Optics Express.*

Prof. Gmachl is a member of the IEEE Photonics Society (formerly the Lasers and Electro-Optics Society) Board of Governors. She is a 2005 MacArthur Fellow and a corresponding member of the Broad of the Austrian Academy of Sciences.